AI4SmallFarms

A Dataset for Crop Field Delineation in Southeast Asian Smallholder Farms

Persello, Claudio; Grift, Jeroen; Fan, Xinyan; Paris, Claudia; Hansch, Ronny; Koeva, Mila; Nelson, Andrew

DOI
10.1109/LGRS.2023.3323095

Publication date
2023

Document Version
Final published version

Published in
IEEE Geoscience and Remote Sensing Letters

Received: 22 March 2023 | Revised: 9 August 2023 | Accepted: 26 September 2023

IET Intelligent Transport Systems

DOI: 10.1049/itr2.12435

The Institution of Engineering and Technology WILEY

ORIGINAL RESEARCH

A risk-based driver behaviour model

Yuxia Yuan[1,2] | Xinwei Wang[3] | Simeon Calvert[1] | Riender Happee[4] | Meng Wang[5]

[1]Department of Transport & Planning, Delft University of Technology, Delft, The Netherlands

[2]Autonomous Aerial Systems, School of Engineering and Design, Technical University of Munich, Ottobrunn, Germany

[3]School of Engineering and Materials Science, Queen Mary University of London, London, UK

[4]Department of Cognitive Robotics, Delft University of Technology, Delft, The Netherlands

[5]Chair of Traffic Process Automation "Friedrich List" Faculty of Transport and Traffic Sciences, Technische Universität Dresden, Dresden, Germany

Correspondence
Meng Wang, Chair of Traffic Process Automation "Friedrich List" Faculty of Transport and Traffic Sciences, Technische Universität Dresden, Hettnerstraße 3, 01069 Dresden, Germany.
Email: meng.wang@tu-dresden.de

Abstract

Current driver behaviour models (DBMs) are primarily designed for the general driver population under specific scenarios, such as car following or lane changing. Hence DBMs capturing individual behaviour under various scenarios are lacking. This paper presents a novel method to quantify individual perceived driving risk in the longitudinal and lateral directions using risk thresholds capturing the time headway and time to line crossing. These are integrated in a risk-based DBM formulated under a model predictive control (MPC) framework taking into account vehicle dynamics. The DBM assumes drivers to operate as predictive controllers jointly optimising multiple criteria, including driving risk, discomfort, and travel inefficiency. Simulation results in car following and passing a slower vehicle demonstrate that the DBM predicts plausible behaviour under representative driving scenarios, and that the risk thresholds are able to reflect individual driving behaviour. Furthermore, the proposed DBM is verified using empirical driving data collected from a driving simulator, and the results show it is able to accurately generate vehicle longitudinal and lateral control matching individual human drivers. Overall, this model can capture individual risk perception behaviour and can be applied to the design and assessment of intelligent vehicle systems.

1 | INTRODUCTION

Modelling driver behaviour is a complex task and it has attracted significant research attention throughout the past decades. A well-developed driver behaviour model (DBM) can not only transfer human driving skills to traffic systems but also help improve current transportation systems' capacity and safety [1]. In this work, we propose an integrated DBM model that has potential applications in various domains. By accurately capturing individual driving behaviour under different driving scenarios, the model can be used to do driving simulations of autonomous vehicles when interacting with human drivers, develop personalised advanced driver assistance systems, and understand human driver behaviours to enhance current traffic systems' safety and efficiency. To develop DBMs, a clear understanding of driver behaviour is essential. Various conceptual theories have been proposed to depict driver behaviour to make driving decisions and interact with other traffic participants [2–4]. According to Michon's theory [2], driver behaviour is reflected at three levels, as shown in Figure 1. General planning stages, like trip goals, routes, and driving models, are defined at the strategic level from a long-term perspective. Controlled action patterns, such as obstacle avoidance and lane selection, are decided at the tactical level, taking up several seconds. Finally, at the operational level, continuous vehicle control is executed. This study focuses on modelling driver behaviour at the operational level.

Driver behaviour at the operational level can be divided into longitudinal (speed) and lateral (steering) control. Typical speed control models include the optimal velocity model (OVM) [5] and the intelligent driver model (IDM) [6]. To address unrealistically large accelerations provided by the OVM, the full velocity difference model (FVDM) was developed [7]. This model took both positive and negative velocity differences into account to enhance velocity control, which improved driving comfort to some degree for car following. Meanwhile, many researchers focused on modelling driver-vehicle lateral control. Weir and McRuer [8] described a basic driver model based on errors in the

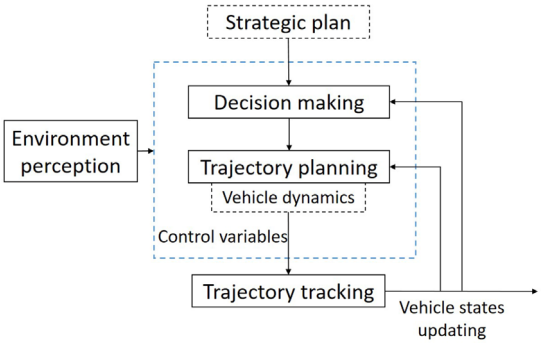

FIGURE 1 The flowchart of vehicle feedback control. This study mainly involves layers circled by dotted blue blocks.

target heading angle and inspired many early studies on steering control. However, most current models are limited to specific driving scenarios, such as car following and lane changes, because they only consider longitudinal speed control or lateral steering control or ignore lateral dynamics. For instance, a driving behaviour analysis using an open dataset was conducted for car-following paired trajectories [9]. To minimise the energy efficiency of electric vehicles, a speed planning model specific for car-following scenarios was developed using model-based reinforcement learning [10]. In addition, a data-driven sequential lane change model was established for lateral control in a spatial domain instead of a traditional temporal domain [11].

Integrated DBMs considering both longitudinal and lateral control have the advantage of adapting to more complex maneuvers [12–14]. A fuzzy logic approach was proposed to model both longitudinal and lateral driver behaviours, aiming to ensure integration between road safety and crash reduction based on an examination of speed limitations under weather conditions [15]. An integrated DBM was formulated as a sequential decision-making problem that is characterised by non-linearity and stochasticity, and unknown underlying cost functions, and an imitation learning approach optimised the formulation [16]. Previous DBM studies have demonstrated that the dynamic bicycle model is a robust description of vehicle dynamics. A hybrid framework [14] utilised the dynamic bicycle model [17] to describe vehicle dynamics. The dynamic bicycle model was also adopted by Prokop to model humans' driving processes as an optimisation problem [13].

Although integrated DBMs are more adaptive for complex driving scenarios, they are not yet realistic in terms of individual real world driving behaviour. For instance, various DBM models immediately correct driving states once the vehicles slightly deviate from a reference path or state [13, 14], which can reduce travel efficiency or cause discomfort in some conditions in practice. In 1981, Gipps proposed a car-following model where the follower response was described based on the expectancy of other vehicles rather than formulating driving velocity directly [18]. In addition, Boer proposed a satisficing driving strategy. It used a time to line crossing (TLC) model to capture driving risk for straight and curved roads [19] as TLC has been proven to be an important indicator to evaluate driver behaviour [20]. Wiedemann defined different thresholds and regimes in the relative speed/space of ego vehicles and their leaders to describe their interaction [21]. The acceleration equations of the Wiedemann model were further modified to represent more realistic driving behaviour, and the model parameters were calibrated using mixed traffic with different conventional vehicle classes [22]. More recently, psychophysical models [23] utilised perceptual thresholds to model driver reactions to changes in driving states. These studies show that thresholds can be used to reflect human driving behaviour regarding safety/risk perception, motion prediction, and speed control.

In this study, we present an innovative approach to address the limitations of current DBMs. For example, some models are not realistic for real world driving or can not reflect individuals' driving preferences. To fill these research gaps, we proposed an integrated risk-based DBM to apply to a range of driving scenarios, where individual driving behaviours are captured by risk-related thresholds. The proposed DBM is derived under a model predictive control (MPC) framework, providing solutions for vehicle control at each sampling time [24]. The dynamic bicycle model, capturing the velocity and steering dynamics of vehicles, is adopted to predict the driving dynamics of ego vehicles on a prediction horizon. To formulate driver behaviour, cost criteria of travel inefficiency, driving risk, and discomfort are defined. These criteria are evaluated by minimising the total cost of six driving objectives (e.g., minimising driving risk, enhancing driving comfort, and improving efficiency in longitudinal and lateral moving directions, respectively). The main contribution of our work lies in proposing a novel method that uses two risk thresholds to measure individual perceived driving risk in the longitudinal and lateral directions, respectively. We verify this approach with empirical data and evaluate the performance of the developed DBM under different driving scenarios.

The remainder of this paper is structured as follows. Section 2 introduces the feedback control framework and model assumptions, and Section 3 provides a detailed description of the proposed DBM. Simulation settings are presented in Section 4, while simulation results and detailed analysis are illustrated in Section 5. In Section 6, the developed DBM is verified using empirical driving data. Finally, Section 7 concludes this paper and discusses potential future research directions.

2 | CONCEPTUAL FRAMEWORK AND MODEL ASSUMPTIONS

In this section, the vehicle feedback control framework and the main assumptions of driver behaviour are introduced.

2.1 | Human driving as feedback control problem

Human driving is a typical feedback control problem [17]. According to the theory proposed by Michon in 1985 [2], the feedback control scheme of human driving is illustrated in

Figure 1. The top layer represents the strategic plan, followed by the decision-making layer, where driving decisions are made based on the current driving states and environment, such as lane selection, desired speed, and duration time of lane changing (LC). Then, the trajectory planning layer generates control commands, including acceleration and steering angle, which are based on the decisions made and take into account the current driving state. Once the corresponding tracking commands are executed, the vehicle updates its driving states, which are then observed by the decision-making and trajectory planning layers to correct their outputs. This cyclical process ensures that the vehicle's actions remain consistent with its intended trajectory.

2.2 | Assumptions of human driver behaviour

Before we formulate the DBM, we state the assumptions on how drivers perceive their driving environment (static and dynamic obstacles), decide on driving objectives, and control their vehicles [25]. The main assumptions of our model include:

- Drivers are predictive controllers:
  Human drivers have the ability to utilise internal models of vehicle dynamics/kinematics to predict the evolution of the local environment based on their previous knowledge or driving experience. Modelling studies [13, 14] showed that average drivers could predict ego vehicles' dynamics as a linear parameter varying system, such as the bicycle vehicle model. Another research [17] indicated that an experienced driver or race driver may be able to predict more complex nonlinear vehicle dynamics for ego vehicles. As for surrounding vehicles, most human drivers could estimate the surrounding vehicles' dynamics using a simpler model. For example, leading vehicles can be assumed to drive on roads with non-zero longitudinal acceleration during car following (CF) maneuvers [14], but keep a constant longitudinal velocity (zero longitudinal acceleration) during lane-changing tasks [26].
- Drivers are optimal and switching controllers:
  Studies indicate that in real driving, there are usually three driving objectives: 1) maximise driving rewards such as travel efficiency and comfort [27]; 2) minimise the cost of control actions, including driving risk, stress, and jerk along trajectories [26], and 3) fulfil constraints like road or lane boundaries that need to hold during the whole driving task [28]. Such objectives shall be jointly addressed by human drivers. For example, a driver who only checks driving rewards may potentially collide with other traffic participants or disrupt traffic flow. In practice, most drivers are able to find an optimal driving strategy to reach their destinations under various driving scenarios. For instance, they might make a trade-off between rewards, cost, and constraints [13, 29]. Moreover, drivers might switch objectives when transitioning from one maneuver to another, since the driving objectives of human controllers are situation-dependent [30].

The proposed integrated risk-based DBM in this study is built upon two fundamental assumptions about driver behaviour: predictive control and optimal/switching control. The first assumption is reflected in the use of an MPC framework for the DBM. This allows the model to predict driver behaviour and adjust to changes in driving conditions. The second assumption, that drivers are optimal controllers, is incorporated into the consideration of three cost criteria: travel inefficiency, driving risk, and discomfort. Meanwhile, drivers' switching abilities are applied to perceive driving risk, where driving risk is formulated by risk thresholds. By minimising the total cost of the three criteria, the DBM is able to generate an optimal driving strategy to complete various driving tasks like humans.

3 | MATHEMATICAL DRIVER BEHAVIOUR MODEL

Human drivers can predict and regulate driving states according to their basic knowledge of vehicle dynamics and driving experience. Focusing on the operational level, this study models driver behaviour under an MPC framework, where the dynamic bicycle model, described in Section 3.1, is used to predict the dynamics of ego vehicles. Control variables $\mathbf{u} = (u_1, u_2)^T$ are optimised to minimise the total cost of driving objectives under dynamic constraints, where u_1 indicates front-wheel steering angle, u_2 represents vehicles' forward acceleration, and T means transpose. Only the first sample of optimal steering and acceleration is used to control vehicles. The control inputs $\mathbf{u}$ are updated at regular intervals, independently bounded by corresponding limitations. Mathematically, the DBM is formulated as an optimisation problem under dynamic equality and inequality constraints:

$$
\begin{aligned}
\mathbf{J}^*(t) = \min_{\mathbf{u}(t)} \quad & J, \quad t \in [t_0, t_0 + t_h] \\
\text{subject to} \quad & \dot{\mathbf{z}}(t) = f(\mathbf{z}(t), \mathbf{u}(t)) \\
& \mathbf{z}(t_0) = \mathbf{z}_c \\
& u_{1.\min} \le u_1(t) \le u_{1.\max} \\
& u_{2.\min} \le u_2(t) \le u_{2.\max}
\end{aligned} \tag{1}
$$

where t_0 is the current time and t_h is the prediction horizon. J represents the cost function that consists of six components, see Section 3.3, which should be minimised by a suitable choice of control variables $\mathbf{u}(t)$.

For the equality constraints, f is the nonlinear dynamics of vehicles (Equation (2)), which is described in Section 3.1. $\mathbf{z}(t_0)$ indicates the initial states of vehicles and corresponds to vehicles' current states, $\mathbf{z}_c$. Meanwhile, control variables should satisfy inequality constraints, indicating that controlled acceleration $u_1(t)$ and steering angle $u_2(t)$ are bound by their limitations. $u_{1.\min}$ indicates the maximum deceleration, $u_{1.\max}$ is the maximum acceleration, and $b_{\min}$ and $b_{\max}$ are the upper and lower boundaries for the steering angle.

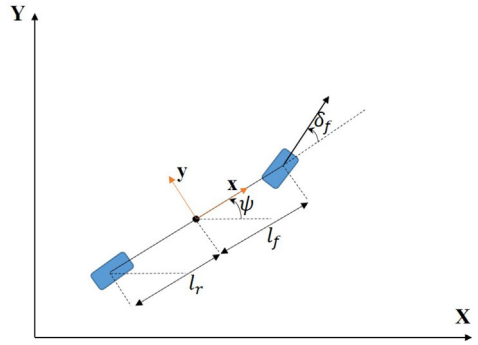

FIGURE 2 The vehicle model. (**X**,**Y**) indicates the global frame, and (x, y) represents the vehicle local frame.

3.1 | The dynamic bicycle model

The dynamic bicycle model is widely used to describe vehicle dynamics [13, 14], offers a realistic representation of forces applied to vehicles, and captures steering dynamics for most lane-based driving scenarios. The model includes dynamic states of the front and rear wheels, merging left and right wheel dynamics. It is also adopted in our study to describe vehicle dynamics as it can be considered an accurate representation of the inference of future states of vehicles in both longitudinal and lateral directions [17], which are requirements for an integrated DBM. We assume linearised lateral tyre slip, making this model suitable for dynamic lateral maneuvers up to around 6 m/s^2.

In Figure 2,(**X**, **Y**) indicates the inertial/global frame, and (**x**, **y**) is used to represent vehicle coordinate systems. The state variables of the dynamic bicycle model are vehicle global position (X, Y), velocity v_x, v_y, heading angle ψ, and corresponding heading angle change rate $\dot{\psi}$, thus defining the state vector $\mathbf{z} = [X, Y, v_x, v_y, \psi, \dot{\psi}]^{\mathrm{T}}$. With the control variable $\mathbf{u}$, the equations of vehicles' motion are given by Equation (2), where $F_i = C_i\alpha_i, i \in \{f, r\}$ is the tire force. f and r denote the front and rear tires, respectively, C_i indicates the cornering stiffness of lumped tires for the axle i, and α_i is the slip angle of lumped tire i. At small angles, α_i can be approximated as: $\alpha_f = \frac{v_y + l_f\dot{\psi}}{v_x} - u_2, \alpha_r = \frac{v_y - l_r\dot{\psi}}{v_x}$ [17].

$$\dot{\mathbf{z}} = \begin{bmatrix} v_x \sin\psi + v_y \cos\psi \\ v_x \cos\psi + v_y \sin\psi \\ v_y\dot{\psi} + u_1 \\ -v_x\dot{\psi} + \frac{F_f}{m} + \frac{F_r}{m} \\ \dot{\psi} + \ddot{\psi}d_t \\ \frac{1}{I_z}\left(l_f F_f - l_r F_r\right) \end{bmatrix} = f(\mathbf{z}, \mathbf{u}) \tag{2}$$

We use (X^e, Y^e), ψ^e, and v_x^e to represent the current global position, heading angle, and driving speed of ego vehicles, and (X^l, Y^l) to denote the position of leading vehicles. Parameters for the dynamic model are listed in Table 1.

TABLE 1 The dynamic bicycle model parameters [14].

Parameters	Default value	Unit	Description
l_f	1.1	m	The distance from the center of gravity to the front axle
l_r	1.58	m	The distance from the center of gravity to the rear axle
C_f	80, 000	N/rad	Front axle cornering stiffness
C_r	80, 000	N/rad	Rear axle cornering stiffness
m	1573	kg	The mass of the vehicle
I_z	2873	kg m^2	Yaw moment of inertia

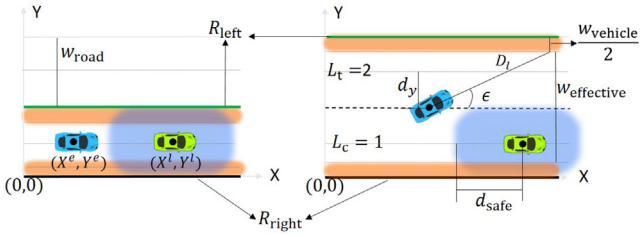

FIGURE 3 The illustration of driving scenarios. The blue vehicle is the ego, and the green one is the leader. The block coloured yellow indicates unreachable areas on the road, and the blue block centered at the leading vehicle is an effective area. (X, Y) indicates the position in the global frame, and w depicts the width (e.g. road, vehicle, and effective area). L_c and L_t are the current and the target driving lanes respectively. R_{left} and R_{right} indicate the left (upper) and right (lower) road boundaries. d_{safe} is the safe front spacing, and d_y represents the lateral position offset. ϵ is the heading angle offset, and D depicts the distance to line crossing.

3.2 | Scenario description

We designed the DBM to capture highway driving, including car following (CF), lane changes (LC) to pass a slower lead vehicle, and free driving. Driving scenarios are illustrated in Figure 3. The left figure shows CF, where the ego vehicle follows the leading vehicle at a safe distance. The right figure indicates the LC process, and after changing lanes, the ego vehicle drives free on the road. We use L_c to indicate the current driving lane and L_t to denote the target lane. The number of lanes is labeled in Figure 3. For L_t, there are two selections: 1) if changing lanes, L_t is the selected target lane; 2) if keeping the current lane, L_t is the same as the current driving lane, L_c.

3.3 | Cost function formulation

By adopting the dynamic bicycle model, the longitudinal and lateral driving states are considered at the same time. However, to develop a DBM, we have to understand how to formulate driver behaviour. We take criteria into consideration, including driving risk, driving inefficiency, and discomfort [13, 14, 26]. These three criteria are evaluated by six driving objectives, including guaranteeing longitudinal and lateral driving safety using risk thresholds, enhancing driving comfort by minimising steering

rate and acceleration rate, and improving driving efficiency by following the desired speed and terminal lateral position.

3.3.1 | Driving risk

Driving risk mainly comes from static obstacles (road boundaries) and dynamic obstacles (other traffic participants). Driver-perceived risk is captured using human drivers' thresholds according to the driving risk concept proposed in [21, 31]. Here, we consider lateral driving risk from lane boundaries and longitudinal driving risk from neighbouring vehicles. If applied to non-lane-based environments, there is no lateral risk coming from lanes.

- Lateral risk:

  Lateral driving risk is measured by the available time to correct driving states using TLC, defined as the time duration available for drivers before crossing any lane boundary. The importance of this indicator for driver performance evaluation and model development is outlined in several research studies [19, 20]. For example, it was successfully applied in satisficing curve negotiation [19]. In this study, we use TLC to evaluate driver perceived lateral risk within straight lanes. According to the concept represented in [31], a threshold of TLC, $\underline{\zeta}$, is defined to reflect an individual acceptable lateral driving risk. When the real TLC is bigger than $\underline{\zeta}$, drivers would like to accept and keep current driving states, while they have to make corrective control actions when the real TLC is smaller than $\underline{\zeta}$.

  When driving on a straight road, we assume that the road parallels the global horizontal axis. θ_r is defined to indicate the angle between the tangent line of a lane and the corresponding global horizontal axis, which is zero for a straight lane. In this way, the TLC on a straight lane is actually infinite when the heading angle parallels the driving lane. Otherwise, the TLC is determined by the non-zero heading angle offset ϵ (Equation (3)) and lateral position offset d_y (Equation (4)). Notice that collision-free driving means any single point of the vehicle does not touch road boundaries or other obstacles. Consequently, the true road width is not an effective driving width for vehicles, and the effective width is calculated taking into account vehicle width w_{vehicle} by Equation (5). Here, the upper road boundary is determined by the results of lane selection, $R_{\text{left}} = w_{\text{road}} L_t$, and the lower boundary is the boundary of the current driving lane, $R_{\text{right}} = w_{\text{road}}(L_c - 1)$.

$$\epsilon = |\theta_r - \psi^e| \tag{3}$$

$$d_y = |(L_t - 1/2)w_{\text{road}} - Y^e| \tag{4}$$

$$w_{\text{effective}} = R_{\text{left}} - R_{\text{right}} - w_{\text{vehicle}} \tag{5}$$

D_l and D_r are used to represent the distance to line crossing for the left and right sides, and ζ_l and ζ_r are corresponding TLC values. The calculation of TLC on a straight road is derived from the Pythagoras theorem. When ψ^e is positive and defined in the counter-clockwise direction, the TLC value ζ_l is calculated by Equations (6) and (7), and ζ_r is calculated by Equations (8) and (9) when ψ^e is negative. Then, the real TLC value ζ is obtained by Equation (10).

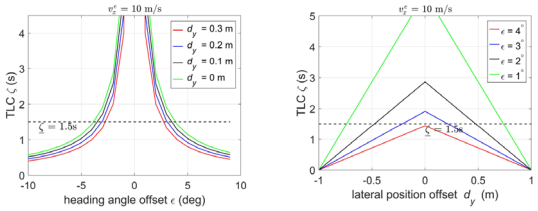

(a) TLC on a straight road for heading angle offsets with specific lateral position offsets.

(b) TLC on a straight road for lateral position offsets with certain heading angles.

FIGURE 4 Effect of lateral position offset and heading angle on ζ on a straight road and corresponding tolerable range for the acceptable TLC.

$$D_l = (w_{\text{effective}}/2 - d_y)/\sin\epsilon \tag{6}$$

$$\zeta_l = D_l / v_x^e \tag{7}$$

$$D_r = (w_{\text{effective}}/2 - d_y)/\sin\epsilon \tag{8}$$

$$\zeta_r = D_r / v_x^e \tag{9}$$

$$\zeta = \begin{cases} \zeta_l, & \text{if } \psi^e \text{ is positive} \\ \zeta_r, & \text{if } \psi^e \text{ is negative} \end{cases} \tag{10}$$

The effects of lateral position offset d_y and heading angle offset ϵ on the value of ζ on a straight road are presented in Figure 4. Here, the current driving velocity is set as v_x^e = 10 m/s, and $L_t = L_c = 0$. The result in Figure 4a indicates that as the heading angle offset increases, the acceptable range of lateral offset decreases, and vice versa. We can also state that the heading angle offset highly affects the value of ζ. From Figure 4b, the acceptable lateral offset is relatively large for a small ϵ (d_y is $\pm$0.25 when $\epsilon = 3°$, but d_y is $\pm$0.75 when $\epsilon = 1°$). It means that even though a vehicle does not follow the center line of the lane, as long as the heading angle offset is small enough, it can still drive safely. In Figure 4, $\underline{\zeta}$ is defined as the individual threshold of ζ according to the concept proposed in [31]. The default value is set at 1.5 s based on the study in [19]. $\underline{\zeta}$ is one of the risk thresholds we adopted to reflect driver behaviour, and the effects of this parameter are simulated and analysed in Section 5.

The lateral driving risk from road constraints can be obtained by comparing the real ζ value with the threshold. Then the Euclidean norm is adopted to evaluate the final driving risk as Equation (11).

$$r_{\text{TLC}} = \int_{t_0}^{t_0+t_h} \|\max(0, \underline{\zeta} - \zeta(t))\|_2 \mathrm{d}t \tag{11}$$

TABLE 2 Simulation parameter settings.

Parameters	Default value	Unit	Description
$u_{1,\max}$	2	m/s^2	Maximum acceleration [32]
$u_{1,\min}$	−4	m/s^2	Maximum deceleration [32]
$u_{2,\max}$	5	deg	Maximum steering angle [35]
$u_{2,\min}$	−5	deg	Minimum steering angle [35]
w_{vehicle}	1.6	m	The width of the vehicle
w_{road}	3.6	m	The width of a single lane
t_h	5	s	The prediction horizon [36]
T_d	5	s	The duration time of LC [36]
τ	1.5	s	The safe headway time [32]
$\underline{\zeta}$	1.5	s	The threshold of TLC [19]
V_{de}	15	m/s	The desired speed
$V^e_{x_0}$	10	m/s	The initial speed of the ego vehicle
$v^l_{x_0}$	13	m/s	The initial speed of the leader
a^l	0	m/s^2	The acceleration of the leader
T_s	8	s	The start time of LC

Parameters for different simulations

Parameters	Car following (CF)	Lane changing (LC)	Effect of $\underline{\zeta}$	Effect of τ
$v^l_{x_0}$	10	-	-	-
a^l	Equation (19)	-	-	-
T_s	Infinity	-	-	-
$\underline{\zeta}$	-	-	[1, 1.5, 2.5, 3]	-
τ	-	-	-	[1, 1.5, 2, 2.5]

- Longitudinal risk:

As for longitudinal driving risk, we only consider the leading vehicle in the driving environment. We use the concept of safe front spacing to quantify longitudinal risk, where the parameter of safe time headway τ is different for individuals [29, 32]. The value of τ affects the interaction between ego vehicles and the leaders, which is measured by the effective area of the leading vehicle, as shown in Figure 3. The width of the effective area is equal to the width of a single lane. The length of this area is determined by the safe front spacing $d_{\text{safe}}(t) = d_0 + \tau v^e_x(t)$, where parameter d_0 is the zero-speed clearance that is set as $d_0 = 5$ m, and τ is the safe time headway that varies between different drivers. The default value of τ is 1.5 s in Table 2. In addition, we will conduct simulations in Section 5 to examine the impact of different values of τ, in order to demonstrate that acceptable safe front spacing for individuals varies depending on different risk thresholds. The analysis will aim to provide insights into how drivers make decisions about safe following distances based on their own perceived level of risk.

The real front spacing between an ego and its leader is calculated by their longitudinal position using Equation (12), where $X^l(t)$ and $X^e(t)$ are the longitudinal positions of the leading vehicle and the ego vehicles at time t. During driving, we assume that the velocity of the leader is within the speed limits on specific roads. Consequently, the ego vehicle approaches the leader at a safe distance to maximise travel efficiency. Then, r_{dis} is calculated using the distance error to reach such goals.

$$d_{\text{real}}(t) = X^l(t) - X^e(t) \tag{12}$$

$$r_{\text{dis}} = \int_{t_0}^{t_0+t_h} \|\max(0, d_{\text{safe}}(t) - d_{\text{real}}(t))\|_2 \mathrm{d}t \tag{13}$$

3.3.2 | Driving comfort and efficiency

In actual driving, drivers try to control vehicles smoothly and comfortably by minimising accelerations and corresponding jerks along the driving directions [26]. Inspired by that, cost functions on the steering angle rate $\dot{u}_2(t)$ and acceleration rate $\dot{u}_1(t)$ are formulated to improve driving comfort, utilising Equations (14) and (15).

$$c_{\text{acc}} = \int_{t_0}^{t_0+t_h} \|\dot{u}_1(t)\|_2 \mathrm{d}t \tag{14}$$

$$c_{\text{angle}} = \int_{t_0}^{t_0+t_h} \|\dot{u}_2(t)\|_2 \mathrm{d}t \tag{15}$$

To improve driving (travel) efficiency and guarantee the completion of LC, terminal driving states are considered. Equation (16) shows the terminal cost for velocity, where $v_x(t_h)$ is the driving speed at time t_h and V_{de} is the desired velocity. Equation (17) formulates the terminal lateral position of ego vehicles to move from the current lane to the target lane or keep the current lane. $Y(t_h)$ is the lateral position of ego vehicles at time t_h. Y_{tar} is the lateral position on the target lane, which is determined by G_{tar} (lane selection).

$$c^{t_h}_{v^e} = \|v_x(t_h) - V_{\text{de}}\|_2 \tag{16}$$

$$c^{t_h}_{Y^e} = \|Y(t_h) - Y_{\text{tar}})\|_2 \tag{17}$$

The final cost function is written as Equation (18), where β_1, β_2, and ... β_6 are weight values for the six cost function components. In this work, the values of β_1, β_2, and ... β_6 are set manually, $\mathbf{fi} = [0.7, 0.2, 2, 2, 1, 0.7]$, to achieve credible results in the scenarios simulated in Section 5. We adopted the method applied in [13, 26], where the key idea is that when the expected cost for a driving objective is too high, the corresponding weight β should be reduced so that the corresponding driving objective costs decrease. By solving this optimisation problem, we can calculate the optimal states of vehicles at each time, that is, the risk-based trajectory for vehicles.

$$J = \beta_1 r_{\text{TLC}} + \beta_2 r_{\text{dis}} + \beta_3 c_{\text{acc}} + \beta_4 c_{\text{angle}} + \beta_5 c^{t_h}_{v^e} + \beta_6 c^{t_h}_{Y^e} \tag{18}$$

3.4 | Problem solution

The proposed DBM is implemented using MPC in a discrete-time form in Matlab. To solve this optimisation problem, we adopt sequential quadratic programming (SQP) as it is a reliable and efficient method to find (local) optimal solutions for both linear and non-linear inequality problems [13, 33]. SQP is particularly suitable for the DBM, which includes several non-linear effects and constraints. The optimal control variables $\mathbf{u}(t)$ are initialised to zero and recalculated at regular time intervals of $t_s = 0.1$ s based on the newest information regarding the system states. The prediction horizon t_h is an important parameter that influences both the computational efficiency and the performance of the DBM. A larger prediction horizon generally leads to better model behaviour but increases computation load. To strike a balance, we set the prediction horizon to $t_h = 5$ s based on previous research presented in [34], where the choice of $t_h = 5$ s was verified as a suitable trade-off between model behaviour and computation load.

4 | SIMULATION SETTINGS

We numerically implement the developed risk-based DBM using discrete-time simulations. The discrete decisions at the tactical layer are set as: the target lane number $L_t = 1$, desired speed $V_{\text{de}} = 15$ m/s, start time of LC $T_s = 8$ s, and duration of LC $T_d = 5$ s. More default parameter settings are listed in Table 1.

We evaluate the performance of the DBM and the sensitivity/effects of risk thresholds on driving behaviour using four separate simulations. The duration of each simulation is 20 s, and it takes around 10 s computation time to optimise two control variables. Hence, this model can be applied online for real-time trajectory planning. The performance of the DBM is evaluated in the first two simulations on a two-lane freeway with a leading vehicle. The sensitivity of risk thresholds is analysed based on the simulation results of using different TLC threshold $\underline{\zeta}$ and safe time headway τ. The four simulations are introduced as follows:

(1) Car following (CF): The first simulation is designed to evaluate the performance of the developed DBM following a non-zero-acceleration leading vehicle. Simulation settings are shown in Table 1. In this simulation, the acceleration of the leading vehicle is set by Equation (19) with an initial velocity $v^l_{x_0} = 10$ m/s. It means the leader accelerates during the first 5 s, decelerates from 5 to 10 s, and then speeds up again until $t = 10$ s. The start time of LC is $T_s = \text{inf.}$, indicating the ego vehicle will not change lanes.

$$a_{lx}(t) = \begin{cases} 1, & \text{if } t \le 5 \\ -0.5, & \text{if } 5 < t \le 10 \\ 0.5, & \text{if } 10 < t \le 15 \\ 0, & \text{if } 15 > t \end{cases} \tag{19}$$

(2) Lane changing (LC): This simulation adopts the default parameters in Table 1 to evaluate the performance of LC.
(3) Effect of $\underline{\zeta}$: The sensitivity/effect of $\underline{\zeta}$ on driving behaviour is evaluated and analysed by applying four different values under CF and LC manoeuvers. In addition, other model parameters are set as default values, as shown in Table 1.
(4) Effect of τ: The sensitivity/effect of τ on driver behaviour is also evaluated and analysed by setting four different values under CF and LC maneuver while setting other parameters as default.

5 | SIMULATION RESULTS

5.1 | Results in car following (CF)

The CF simulation result in Figure 5a is the generated trajectory, while Figure 5b shows the driving heading angle, and Figure 5c depicts the controlled steering angle. These figures show that the developed integrated DBM completes CF successfully. During CF, the driving direction of the ego vehicle is always parallel to the driving lane. Since the simulated driving scenario is set on a straight road, the heading angle and steering angle remain zero, as well as the steering angle rate ϵ_{angle} in Figure 6c. Meanwhile, TLC value $\underline{\zeta}$ is infinite in Figure 6a resulting in lateral driving risk also being zero.

Figure 5d shows the front longitudinal spacing between the ego vehicle and the leader. Figure 5e depicts the speed of the ego vehicle and the leading vehicle. The velocity of the leading vehicle is determined by the initial value $v^l_{x_0} = 10$ m/s and the acceleration (the dashed line in Figure 5f). From Figure 5d,e, we can see that when the leading vehicle accelerates/decelerates suddenly, the ego vehicle can change velocity in a timely manner to keep a safe front spacing while guaranteeing driving comfort without a significant change in acceleration (Figure 5f). The ego vehicle accelerates at the first five seconds to maximise efficiency by reducing front spaicng r_{dis} (Figure 6d) and increasing driving velocity (Figure 6e). As the leading vehicle slows down, the longitudinal driving risk increases, forcing the ego vehicle to decelerate. Finally, the ego reaches the desired velocity $V_{\text{de}} = 15$ m/s where the velocity offset (Figure 6e), longitudinal risk (Figure 6d), and longitudinal jerk become zero (Figure 6f). Note that even though the velocity offset is relatively large at first in Figure 6e, it does not heavily affect the current driving states ($t_h = 5$ s). In additional simulations, a maximum deceleration of 6 m/s^2 has been set for the leading vehicle. Results demonstrate that the developed model performs effectively when the leading vehicle brakes suddenly by giving a high penalty to the terminal cost for the desired velocity.

5.2 | Results in lane changing (LC)

Figure 7 shows the simulated lateral and longitudinal dynamics for CF and LC maneuvers, and Figure 8 represents six components in the cost function. Figure 7a is the generated trajectory;

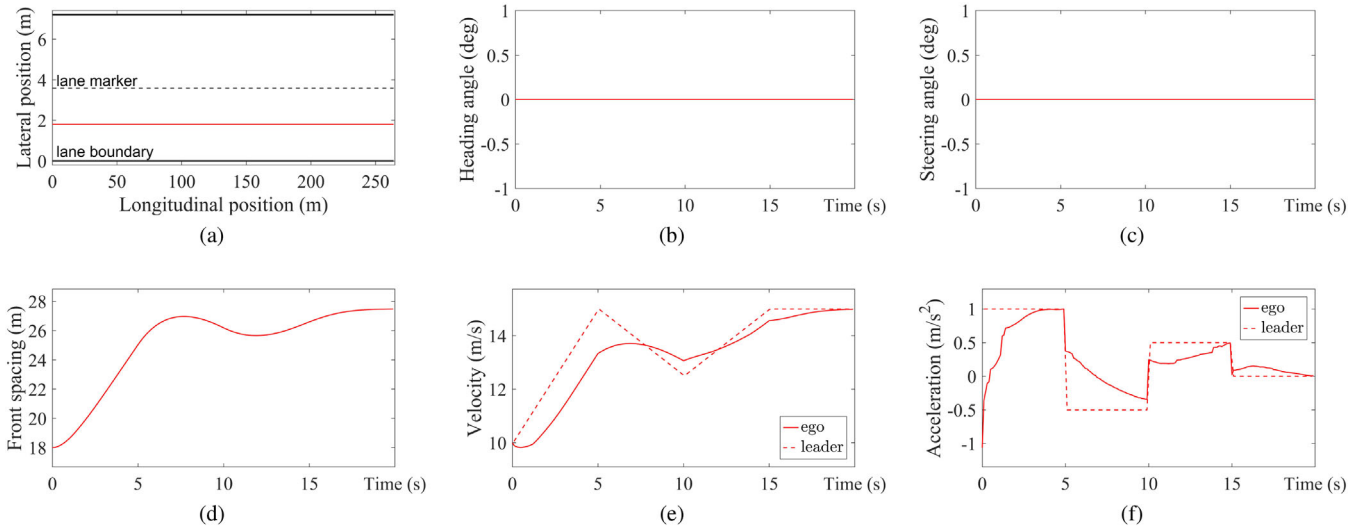

FIGURE 5 Simulated lateral and longitudinal dynamics during CF, following a non-zero-acceleration leading vehicle. The solid line in (a) is the generated trajectory, (b) is heading angle, (c) is steering angle, and (d) depicts front spacing. (e,f) Driving velocity and acceleration of the ego vehicle and its leading vehicle.

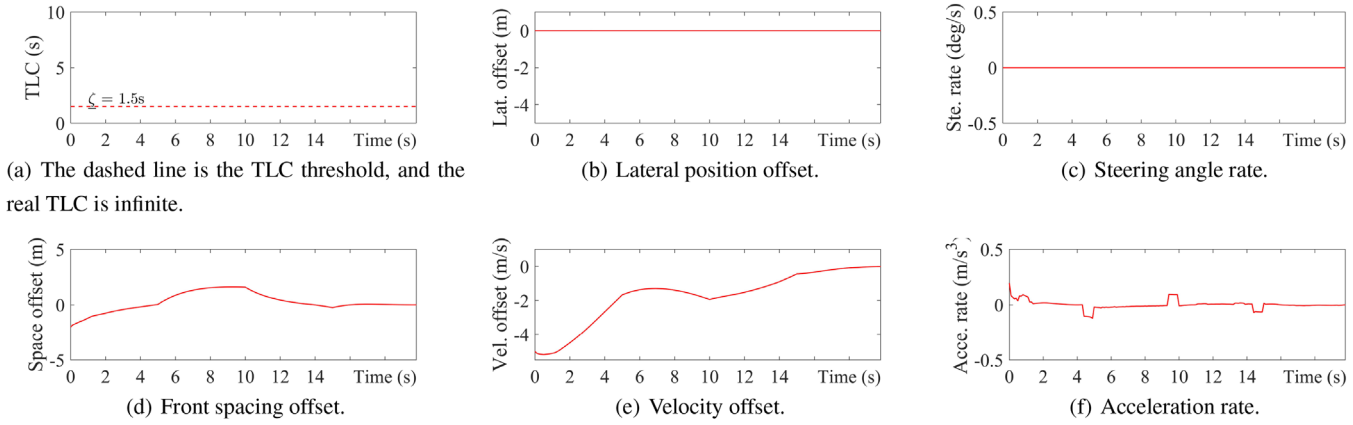

FIGURE 6 The six components of the cost function during CF. Lat., Ste,. Vel., and Acce. are the abbreviations of Lateral, Steering, Velocity, and Acceleration.

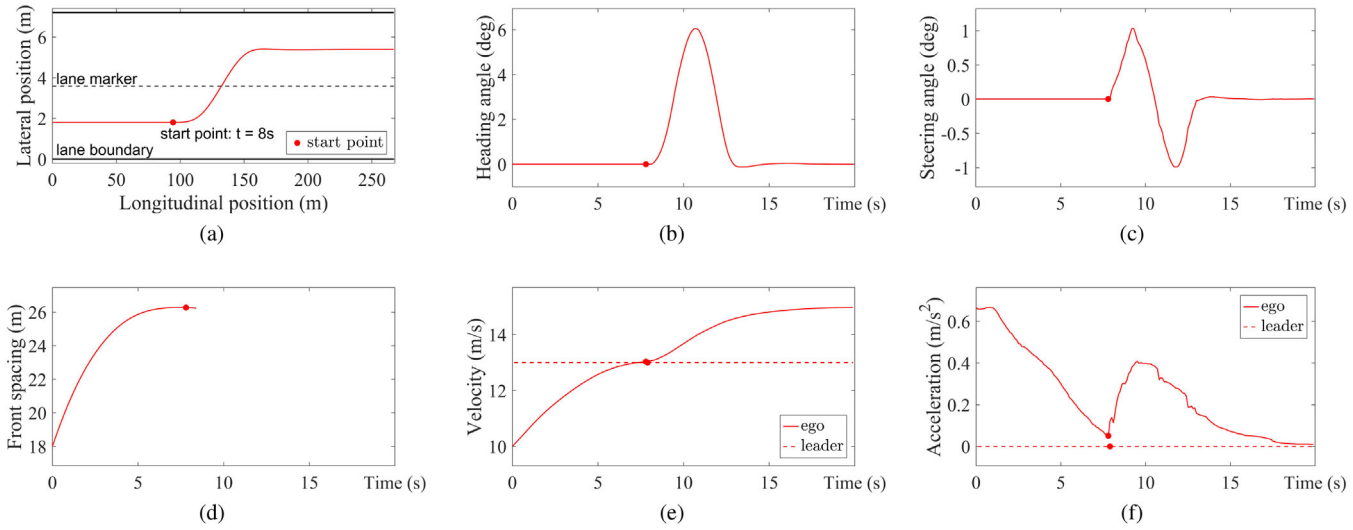

FIGURE 7 Simulated lateral and longitudinal dynamics during CF and LC maneuver. The solid line in (a) is the generated trajectory, (b) is heading angle, (c) is steering angle, and (d) depicts front spacing during CF. (e,f) Driving velocity and acceleration of the ego vehicle and its leading vehicle.

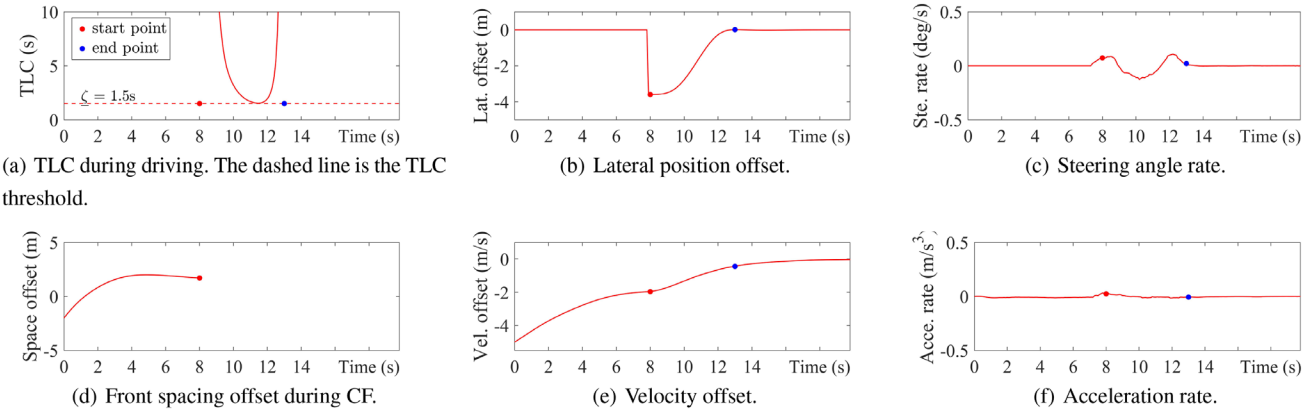

(a) TLC during driving. The dashed line is the TLC threshold.
(b) Lateral position offset.
(c) Steering angle rate.
(d) Front spacing offset during CF.
(e) Velocity offset.
(f) Acceleration rate.

FIGURE 8 The six components of the cost function during CF and LC maneuver. Lat., Ste., Vel., and Acce. are the abbreviations of Lateral, Steering, Velocity, and Acceleration.

Figure 7b shows the driving heading angle, and Figure 7c depicts the controlled steering angle. From Figure 7a and the TLC value in Figure 8a, we can see that the ego vehicle performs CF and LC tasks while keeping the real TLC ζ above the TLC threshold $\underline{\zeta}$. During LC, ζ decreases gradually, indicating increased lateral driving risk. When the heading angle peaks (Figure 7b), the TLC value ζ equals $\underline{\zeta}$. As the ego vehicle approaches the target lane, the TLC gets far away from the TLC threshold again. The same as the effect of velocity offset mentioned before, a large lateral position offset in Figure 8b affects the current driving states slightly. The lateral position offset is close to zero with the reduction of heading angle.

The front spacing between the ego vehicle and the leader is depicted in Figure 7d. After changing lanes, the ego vehicle and the previous leading vehicle drive on different lanes, so this figure only shows the front spacing when they are on the same lane, where the red point indicates the start time of LC. Figure 7e,f denotes the driving velocity and the controlled acceleration of the ego and the leader. From Figure 7f, the ego vehicle speeds up at a relatively large acceleration until the front distance approaches the safe driving distance, where r_{dis} equals zero (Figure 8d). Then the ego vehicle increases its velocity slowly to follow the leading vehicle's speed $v_l = 13$ m/s. After changing lanes, the ego vehicle does not need to keep a large front spacing with the leader. It accelerates to reach the desired velocity (Figure 8e). In addition, the optimised steering angle rate and acceleration rate shown in Figure 8c,f indicate that the driving comfort is enhanced.

5.3 | Results of effect of $\underline{\zeta}$

Simulation results in Figure 9a show the generated trajectories. Figure 9b,c presents heading angle and controlled steering angle. From these two figures, we can see that $\underline{\zeta}$ highly affects lateral/steer control. A large $\underline{\zeta}$ makes the model very sensitive. The reason is that when a driver tries to minimise lateral risk r_{TLC}, she/he has to reduce speed, heading angle offset or lateral position offset as we analysed in Section 3.3.1. Because lateral position and velocity are also related to terminal cost and longitudinal driving risk, the driver would like to minimise heading angle offset. On the other hand, Figure 9d,e,f indicates that $\underline{\zeta}$ has little influence on longitudinal control. In our test case, the DBM performs well by setting $\underline{\zeta}$ between 1 and 2.5. However, to guarantee driving safety, we suggest a range of $\underline{\zeta} \in [1.5, 2.5]$.

5.4 | Results of effect of τ

Simulation results of the effects of τ are shown in Figure 10. The results of heading angle (Figure 10b) and steering angle (Figure 10c) indicates that the safe time headway affects lateral control slightly. Setting the initial front spacing between the ego vehicle and the leading vehicle as a constant value, a smaller τ forces the ego to drive closer to the leader, according to Figure 10d,e. Consequently, the ego vehicle becomes more sensitive to changes in front spacing. Meanwhile, we can see that a large τ pushes the ego to decelerate abruptly at first from Figure 10f. Furthermore, a large driving distance between the leader and the follower yields low travel efficiency and decreases road capability, even though it can improve driving safety to some degree. A reasonable range of τ is between 1.5 and 2 s where 1.5 s is the minimum value to avoid collisions with leading vehicles [32]. To guarantee travel efficiency and improve transportation capacity, we suggest a maximum of τ as 2 s based on the simulation results of the effect of τ.

6 | MODEL VERIFICATION WITH EMPIRICAL DATA

In this section, we verify the proposed risk-based DBM using empirical observations to test its reliability when applied to real driving. Since two risk thresholds are used to reflect individual driving behaviours, they are calibrated using part of the empirical driving data, in Section 6.1, according to Equations (11) and (13). The calibrated parameters are given in Table 3.

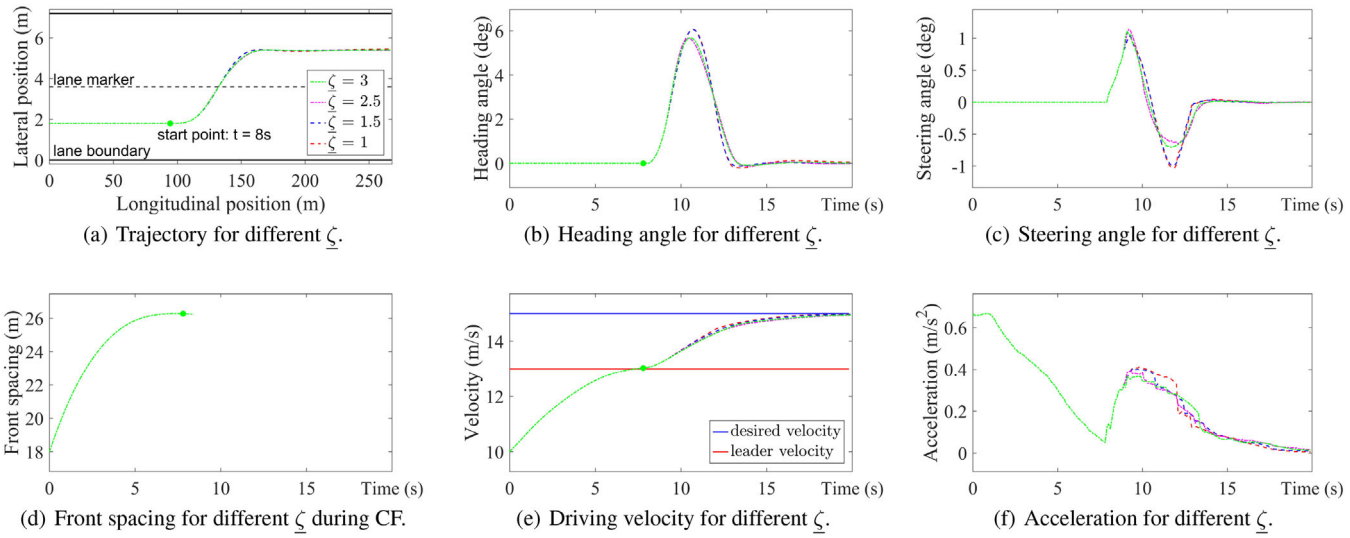

FIGURE 9 Simulated lateral and longitudinal dynamics using different $\underline{\zeta}$. (d) depicts the front spacing when the ego vehicle and leading vehicle drive on the same lane. The solid red line in (e) is the speed of the leading vehicle, and the solid blue one depicts the desired velocity. The dots in the figure indicate the start time of LC.

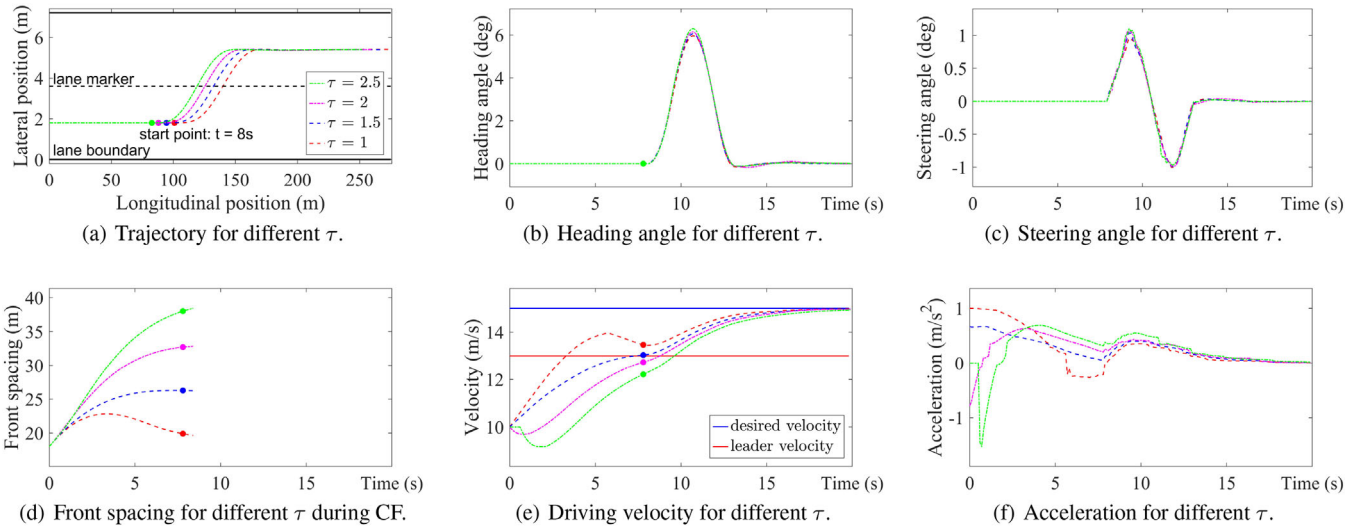

FIGURE 10 Simulated lateral and longitudinal dynamics using different τ values. (d) depicts the front spacing when the ego vehicle and leading vehicle drive on the same lane. The solid red line in (e) is the speed of the leading vehicle, and the solid blue one depicts the desired velocity. The dots in the figure indicate the start time of LC.

TABLE 3 Parameters calibrated using empirical data.

	TLC threshold $\underline{\zeta}$	Safe headway time τ
Driver 1	1.6	1.6
Driver 2	2.4	1.6

6.1 | Empirical driving data

We use an empirical driving dataset collected by a driving simulator based on PreScan to verify the developed model [37]. The dataset recorded the driving data of two different drivers on a two-lane road with normal traffic conditions (no crashes). Each driver was instructed to conduct a CF manoeuver during the first 9 s, and then start LC while decreasing the driving velocity. There is a leading vehicle during CF and no vehicle in the target lane. The experiment was repeated ten times by each driver. Each sample contained the current position, heading angle, velocity, acceleration, and steering angle of ego vehicles, and the position of leading vehicles, captured at 10 Hz. Considering this dataset was collected in CF and LC scenarios, and recorded detailed trajectory information of ego vehicles and the position information of leaders, it is suitable for us to verify our

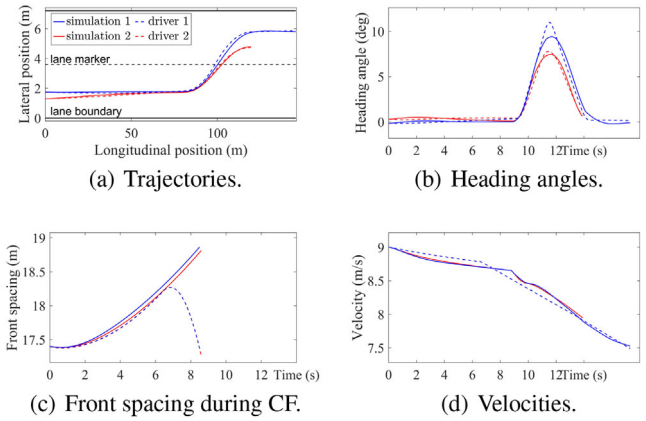

(a) Trajectories. (b) Heading angles.

(c) Front spacing during CF. (d) Velocities.

FIGURE 11 Validation experiments using driving data from two different drivers. The blue and red dashed lines indicate observations from driver 1 and driver 2, respectively. The solid lines coloured blue and red are the outputs of the developed DBM.

model with empirical data. The desired tactical decisions in this dataset are set using the closest values, such as when the desired velocity during CF is set as $V_{\text{de}} = 9$ m/s, which is changed to $V_{\text{de}} = 7.5$ m/s after starting LC, where $L_c = 1$ and $L_f = 2$.

6.2 | Results analysis

Applying the parameters obtained from empirical observations to DBM in Section 3, simulation results are shown in Figure 11. The dashed lines in Figure 11 show the observed trajectories for driver 1 and driver 2, and solid lines are the outputs of DBM, where the model parameters are adapted based on the observations of each driver as shown in Table 3. From Figure 11a, we can see that both the drivers and the developed DBM can track the lane center during CF. After changing lanes, the observations do not follow the lane center closely. It implies that the perceived risk for human drivers is acceptable, not requiring any corrective action to track the lane center line. Meanwhile, the developed DBM performs similarly, which indicates our developed model is able to behave like human drivers by using TLC thresholds to evaluate lateral driving risk. The performance of our model is also supported by the result shown in Figure 11b, where the maximum heading angle of driver 1 is larger than that of driver 2. The reason could be that the TLC threshold of driver 1 is smaller than that of driver 2 (in Table 1). The effects of the TLC threshold on driving behaviours are consistent with the simulation results in Figure 9b. Figure 11d,c shows that our model keeps a safe distance from leading vehicles like humans by changing driving speed. Results indicate that the developed model is able to behave like human drivers, driving safely and efficiently. In addition, by minimising acceleration, steering angle, and their changing rates, driving comfort has been enhanced [38]. Meanwhile, two risk thresholds function well to reflect how each driver perceives longitudinal and lateral driving risk.

7 | CONCLUSIONS

We have developed an integrated risk-based DBM under an MPC framework, that adopts the dynamic bicycle model to predict ego vehicle dynamics. This model operates at the control level in a feedback loop, taking into account driving risk from road and lane boundaries and neighbouring vehicles, while simultaneously enhancing travel efficiency and driving comfort by minimising corresponding costs. Four simulations are designed to evaluate the performance of the developed DBM and analyse the effects of risk thresholds on driving behaviour. The first two simulations demonstrate that our model performs exceptionally well during CF and LC maneuvers. These results showcase the advantages of our integrated DBM, which can generate smooth and comfortable trajectories and adapt to various driving scenarios. Simulations 3 and 4 analyse the sensitivity of risk thresholds and the effects of various parameter settings on driving behaviour. The results demonstrate that the choice of threshold values has a modest impact on the driving behaviour of the model. We also provide reference ranges for two risk thresholds based on our simulation results. Finally, we verify that the developed model is able to behave like humans using empirical data, especially for driving risk evaluation. In conclusion, our integrated risk-based DBM has demonstrated promising results, indicating that it could be applied to intelligent traffic systems to help enhance driving safety, efficiency, and comfort. The sensitivity analysis of risk thresholds provides valuable insights into their influence on driving behaviour. A limitation of our study is that a tactical-decision model is not integrated, so some decisions are manually given, such as the start of the lane change. To address this issue, we plan to incorporate a risk-based decision-making model into future studies. In this case, this integrated DBM can be applied to more driving scenarios including non-lane based environment. Meanwhile, we will use more empirical driving data, including videography data, to verify our findings and models.

AUTHOR CONTRIBUTIONS

Yuxia Yuan: Conceptualization, methodology, resources, software, validation, visualization, writing - original draft. Xinwei Wang: Conceptualization, writing - review and editing. Simeon Calvert: Writing - review and editing. Riender Happee: Conceptualization, methodology, supervision, writing - review and editing. Meng Wang: Conceptualization, methodology, supervision, writing - review and editing.

ACKNOWLEDGEMENTS

Open access funding enabled and organized by Projekt DEAL.

CONFLICT OF INTEREST STATEMENT

The authors declare no conflicts of interest.

DATA AVAILABILITY STATEMENT

The data that support the findings of this study are available from the corresponding author upon reasonable request.

ORCID

Yuxia Yuan https://orcid.org/0000-0003-3565-6993

REFERENCES

1. Xu, Q., Hedrick, K., Sengupta, R., VanderWerf, J.: Effects of vehicle-vehicle/roadside-vehicle communication on adaptive cruise controlled highway systems. In: Proceedings IEEE 56th Vehicular Technology Conference. Vol. 2, pp. 1249–1253. IEEE, Piscataway, NJ (2002). http://ieeexplore.ieee.org/document/1040805/
2. Michon, J.A.: A critical view of driver behavior models: What do we Know, what should we do? In: Human Behavior and Traffic Safety, pp. 485–524. Springer, US (1985). http://link.springer.com/10.1007/978-1-4613-2173-6_19
3. Rasmussen, J.: Skills, rules, and knowledge; signals, signs, and symbols, and other distinctions in human performance models. IEEE Trans. Syst. Man Cybern. 13(3), 257–266 (1983). https://ieeexplore.ieee.org/abstract/document/6313160 http://ieeexplore.ieee.org/document/6313160/
4. Fuller, R.: Towards a general theory of driver behaviour. Accid. Anal. Prev. 37(3), 461–472 (2005). https://linkinghub.elsevier.com/retrieve/pii/S0001457505000102
5. Bando, M., Hasebe, K., Nakayama, A., Shibata, A., Sugiyama, Y.: Dynamical model of traffic congestion and numerical simulation. Phys. Rev. E. 51(2), 1035–1042 (1995). https://link.aps.org/doi/10.1103/PhysRevE.51.1035
6. Treiber, M., Hennecke, A., Helbing, D.: Congested traffic states in empirical observations and microscopic simulations. Phys. Rev. E 62(2), 1805–1824 (2000). https://link.aps.org/doi/10.1103/PhysRevE.62.1805
7. Jiang, R., Wu, Q., Zhu, Z.: Full velocity difference model for a car-following theory. Phys. Rev. E 64(1), 017101 (2001). https://link.aps.org/doi/10.1103/PhysRevE.64.017101
8. Weir, D.H., McRuer, D.T.: Dynamics of driver vehicle steering control. Automatica 6(1), 87–98 (1970). https://linkinghub.elsevier.com/retrieve/pii/0005109870900774
9. Hu, X., Zheng, Z., Chen, D., Zhang, X., Sun, J.: Processing, assessing, and enhancing the Waymo autonomous vehicle open dataset for driving behavior research. Transp. Res. Part C Emerging Technol. 134, 103490 (2022).
10. Lee, H., Kim, K., Kim, N., Cha, S.W.: Energy efficient speed planning of electric vehicles for car-following scenario using model-based reinforcement learning. Appl. Energy 313, 118460 (2022).
11. Gao, J., Murphey, Y.L., Yi, J., Zhu, H.: A data-driven lane-changing behavior detection system based on sequence learning. Transportmetrica B: Transport Dyn. 10(1), 831–848 (2022).
12. Tian, H., Wei, C., Jiang, C., Li, Z., Hu, J.: Personalized lane change planning and control by imitation learning from drivers. IEEE Trans. Ind. Electron. 70(4), 3995–4006 (2023). https://ieeexplore.ieee.org/document/9786545/
13. Prokop, G.: Modeling human vehicle driving by model predictive online optimization. Veh. Syst. Dyn. 35(1), 19–53 (2001).http://www.tandfonline.com/doi/abs/10.1076/vesd.35.1.19.5614
14. Mullakkal-Babu, F.A., Wang, M., van Arem, B., Shyrokau, B., Happee, R.: A hybrid submicroscopic-microscopic traffic flow simulation framework. IEEE Trans. Intell. Transp. Syst. 22(6), 3430–3443 (2021).https://ieeexplore.ieee.org/document/9088249/
15. Almadi, A.I., Al Mamlook, R.E., Almarhabi, Y., Ullah, I., Jamal, A., Bandara, N.: A fuzzy-logic approach based on driver decision-making behavior modeling and simulation. Sustainability 14(14), 8874 (2022).
16. Bhattacharyya, R., Wulfe, B., Phillips, D.J., Kuefler, A., Morton, J., Senanayake, R., et al.: Modeling human driving behavior through generative adversarial imitation learning. IEEE Trans. Intell. Transp. Syst. 24(3), 2874–2887 (2022)
17. Rajamani, R.: Vehicle dynamics and control. Mechanical Engineering Series. Springer US (2012). https://link.springer.com/10.1007/978-1-4614-1433-9
18. Gipps, P.G.: A behavioural car-following model for computer simulation. Transportation Research Part B: Methodological 15(2), 105–111 (1981). Transp. Res. Part B Methodol. https://linkinghub.elsevier.com/retrieve/pii/0191261581900370
19. Boer, E.R.: Satisficing curve negotiation: Explaining drivers' situated lateral position variability. IFAC PapersOnLine 49(19), 183–188 (2016). https://www.sciencedirect.com/science/article/pii/S2405896316320730
20. Mammar, S., Glaser, S., Netto, M.: Time to line crossing for lane departure avoidance: A theoretical study and an experimental setting. IEEE Trans. Intell. Transp. Syst. 7(2), 226–241 (2006). http://ieeexplore.ieee.org/document/1637677/
21. Misbah, S., Hassan, H., Yusof, M.Y., Hanifah, Y.A., AbuBakar, S.: Genomic species identification of Acinetobacter of clinical isolates by 16S rDNA sequencing. Singapore Med. J. 46(9), 461–464 (2005). http://www.ncbi.nlm.nih.gov/pubmed/16123830
22. Anil Chaudhari, A., Srinivasan, K.K., Rama Chilukuri, B., Treiber, M., Okhrin, O.: Calibrating Wiedemann-99 model parameters to trajectory data of mixed vehicular traffic. Transp. Res. Rec. 2676(1), 718–735 (2022)
23. Ahmed, H.U., Huang, Y., Lu, P.: A review of car-following models and modeling tools for human and autonomous-ready driving behaviors in micro-simulation. Smart Cities 4(1), 314–335 (2021). https://www.mdpi.com/2624-6511/4/1/19
24. Cao, W., Mukai, M., Kawabe, T., Nishira, H., Fujiki, N.: Mild merging path generation method with optimal merging point based on MPC. IFAC Proc. Vol. 46(21), 756–761 (2013). https://linkinghub.elsevier.com/retrieve/pii/S1474667016384658
25. Hoogendoorn, S., Hoogendoorn, R., Wang, M., Daamen, W.: Modeling driver, driver support, and cooperative systems with dynamic optimal control. Transp. Res. Rec. 2316(1), 20–30 (2012). https://journals.sagepub.com/doi/10.3141/2316-03
26. Kuderer, M., Gulati, S., Burgard, W.: Learning driving styles for autonomous vehicles from demonstration. In: 2015 IEEE International Conference on Robotics and Automation (ICRA), pp. 2641-2646. IEEE, Piscataway, NJ (2015). http://ieeexplore.ieee.org/document/7139555/
27. Ben-Asher, J.Z., Rimon, E.D.: Time optimal trajectories for a car-like mobile robot. IEEE Trans. Rob. 38(1), 421–432 (2022). https://ieeexplore.ieee.org/document/9451188/
28. Werling, M., Kammel, S., Ziegler, J., Gröll, L.: Optimal trajectories for time-critical street scenarios using discretized terminal manifolds. Int. J. Rob. Res. 31(3), 346–359 (2012). http://journals.sagepub.com/doi/10.1177/0278364911423042
29. Wang, M., Hoogendoorn, S.P., Daamen, W., van Arem, B., Happee, R.: Game theoretic approach for predictive lane-changing and car-following control. Transp. Res. Part C Emerging Technol. 58, 73–92 (2015). https://linkinghub.elsevier.com/retrieve/pii/S0968090X15002491
30. Kolekar, S., de Winter, J., Abbink, D.: Human-like driving behaviour emerges from a risk-based driver model. Nat. Commun. 11(1), 4850 (2020). https://www.nature.com/articles/s41467-020-18353-4
31. Näätänen, R., Summala, H.: Road-User Behaviour and Traffic Accidents. North-Holland Publishing Company, Amsterdam (1976). https://trid.trb.org/view/46118
32. Zhang, J., Li, Q., Chen, D.: Integrated adaptive cruise control with weight coefficient self-tuning strategy. Appl. Sci. 8(6), 978 (2018). http://www.mdpi.com/2076-3417/8/6/978
33. Andrei, N.: A SQP algorithm for large-scale constrained optimization: SNOPT. In: Springer Optimization and Its Applications. Vol. 121, pp. 317–330. Springer International Publishing, Berlin (2017). http://link.springer.com/10.1007/978-3-319-58356-3_15
34. Wang, M., Daamen, W., Hoogendoorn, S.P., van Arem, B.: Driver assistance systems modeling by model predictive control. In: 2012 15th International IEEE Conference on Intelligent Transportation Systems, pp. 1543–1548. IEEE, Piscataway, NJ (2012). http://ieeexplore.ieee.org/document/6338824/
35. Rajvardhan, R.P., Shankapal, S.R., Vijaykumar, S.M.: Effect of wheel geometry parameters on vehicle steering. SAS Tech J. 9(2), 592–597 (2010). Available from: https://www.indianjournals.com/ijor.aspx?target=ijor:sastech&volume=9&issue=2&article=002
36. Toledo, T., Zohar, D.: Modeling duration of lane changes. Transp. Res. Rec. 1999(1), 71–78 (2007). http://journals.sagepub.com/doi/10.3141/1999-08

37. Lu, C., Hu, F., Cao, D., Gong, J., Xing, Y., Li, Z.: Transfer learning for driver model adaptation in lane-changing scenarios using manifold alignment. IEEE Trans. Intell. Transp. Syst. 21(8), 3281–3293 (2020). https://ieeexplore.ieee.org/document/8759907/
38. Zheng, Y., Shyrokau, B., Keviczky, T.: 3DOP: Comfort-oriented motion planning for automated vehicles with active suspensions. In: 2022 IEEE Intelligent Vehicles Symposium (IV), pp. 390–395. IEEE, Piscataway, NJ (2022)

How to cite this article: Yuan, Y., Wang, X., Calvert, S., Happee, R., Wang, M.: A risk-based driver behaviour model. IET Intell. Transp. Syst. , 1–13 (2023). https://doi.org/10.1049/itr2.12435